# Changes in the Relative Occupancy of Metal-Binding Sites in the Profile Structure of the Sarcoplasmic Reticulum Membrane Induced by Phosphorylation of the $Ca^{2+}$ATPase Enzyme in the Presence of Terbium: A Time-Resolved, *Resonance* X-Ray Diffraction Study

Francisco J. Asturias, Robert F. Fischetti,* and J. Kent Blasie
Department of Chemistry, University of Pennsylvania, and *Biostructures Institute, University City Science Center, Philadelphia, Pennsylvania 19104 USA

ABSTRACT Time-resolved, terbium resonance x-ray diffraction experiments have provided the locations of three different high-affinity metal-binding/transport sites on the $Ca^{2+}$ATPase enzyme in the profile structure of the sarcoplasmic reticulum (SR) membrane. By considering these results in conjunction with the known, moderate-resolution profile structure of the SR membrane (derived from nonresonance x-ray and neutron diffraction studies), it was determined that the three metal-binding sites are located at the "headpiece/stalk" junction in the $Ca^{2+}$ATPase profile structure, in the "transbilayer" portion of the enzyme profile near the center of the membrane phospholipid bilayer, and at the intravesicular surface of the membrane profile. All three metal-binding sites so identified are simultaneously occupied in the unphosphorylated enzyme conformation. Phosphorylation of the ATPase causes a redistribution of metal density among the sites, resulting in a net movement of metal density toward the intravesicular side of the membrane, i.e., in the direction of calcium active transport. We propose that this redistribution of metal density is caused by changes in the relative binding affinities of the three sites, mediated by local structural changes at the sites resulting from the large-scale (i.e., long-range) changes in the profile structure of the $Ca^{2+}$ATPase induced by phosphorylation, as reported in an accompanying paper. The implications of these results for the mechanism of calcium active transport by the SR $Ca^{2+}$ATPase are discussed briefly.

## INTRODUCTION

The sarcoplasmic reticulum (SR) membrane is among the most widely studied and best characterized biologically active ion-transport systems (Inesi, 1985). However, little is known about the mechanism by which the $Ca^{2+}$ATPase, an integral membrane protein, performs the active transport of calcium across the SR membrane (Meissner and Fleischer, 1974). This is certainly due, at least in part, to the lack of a high-resolution, three-dimensional structure for the enzyme. X-ray and neutron diffraction studies have provided the moderate resolution, cylindrically averaged profile structure of the $Ca^{2+}$ATPase within the isolated SR membrane (Herbette et al., 1985), and have characterized the changes in the enzyme's profile structure that occur upon $Ca^{2+}$-activated phosphorylation of the protein (Blasie et al., 1985, Pascolini et al., 1988). $La^{3+}$ resonance x-ray diffraction studies (Asturias and Blasie, 1991) have identified the positions in the SR membrane profile of two high-affinity metal-binding/transport sites for the unphosphorylated ($M_xE$)[1] conformation of the enzyme, an important first step toward the elucidation of the ion transport mechanism; these sites were located at the junction of the "headpiece/stalk" and at the intravesicular surface regions of the $Ca^{2+}$ATPase profile structure.

We have now extended our lanthanide resonance x-ray diffraction work to include the first essential step of the active calcium transport process, enzyme phosphorylation and the "occlusion" of the bound metal ions ($M_xE \rightarrow M_xE \sim P$). As preparation for the time-resolved, resonance x-ray diffraction work, biochemical studies were undertaken to measure the effect of lanthanides on the extent of enzyme phosphorylation and phosphoenzyme lifetime, under the conditions that would be necessary for the time-resolved, resonance x-ray diffraction work. We found that lanthanides are capable of activating phosphorylation of the ATPase, resulting in substantial levels of phosphoenzyme, and that the lifetime of the phosphoenzyme formed in the presence of lanthanides at a low temperature of ~4°C is long enough (20–60 min) to allow for the collection of sufficiently accurate resonance x-ray diffraction data. Furthermore, based on a number of considerations (see Asturias et al., 1993), we decided to use terbium as the calcium analog for the x-ray diffraction work. Time-resolved, *nonresonance* x-ray diffraction studies were undertaken to determine whether any changes in the profile structure of the ATPase protein occur upon $Tb^{3+}$-activated enzyme phosphorylation. Significant structural changes were found upon $Tb^{3+}$-activated phosphorylation of the $Ca^{2+}$ATPase, and they were similar in nature, but smaller in magnitude, to those found upon $Ca^{2+}$-activated enzyme phosphorylation. The results from these biochemical/kinetic

[1] The $M_xE$ (or $M_xE\sim P$) is used to indicate which metal is occupying the binding/transport sites on the $Ca^{2+}$ATPase, and activating the enzyme for phosphorylation. $M_xE\sim P$ represents the phosphorylated enzyme conformation. We have purposely chosen not to indicate a particular binding stoichiometry (see Discussion).

*Received for publication 29 January 1993 and in final form 16 February 1994.*

Address reprint requests to J. Kent Blasie, Department of Chemistry, Chemistry Building, University of Pennsylvania, Philadelphia, PA 19104-6323. Tel.: 215-898-6208; Fax: 215-898-6242.



0006-3495/94/05/1665/13 $2.00

studies and time-resolved, nonresonance x-ray diffraction studies are described in an accompanying paper (Asturias et al., 1994).

Backed by the results summarized above, we proceeded to perform the time-resolved, $Tb^{3+}$ resonance x-ray diffraction experiments. The results described in the present paper indicate that, in addition to the two high-affinity metal-binding/transport sites previously identified by our $La^{3+}$ resonance diffraction study of the $Ca^{2+}$ATPase, there is a third site occupied by $Tb^{3+}$ located near the center of the phospholipid bilayer region of the SR membrane profile structure, which seems to be the highest affinity metal-binding/transport site and occurs within the "transbilayer" portion of the enzyme. We also determined that terbium-activated phosphorylation of the ATPase causes a significant redistribution of metal density among the three identified metal-binding sites, in a manner that provides direct evidence concerning the possible nature of the calcium transport mechanism in this prototypical, active ion-transport membrane system.

## METHODS AND DATA ANALYSIS

The methods and procedures used for the preparation of the hydrated, oriented multilayer specimens of isolated SR membranes, the collection of their lamellar x-ray diffraction data, and initial diffraction data reduction are described in an accompanying paper (Asturias et al., 1994), and will not be presented here. The result of the first phase of data reduction were sets of three background scattering-corrected, lamellar intensity functions $I_c(z^*, E_{edge})$, and $I_c(z^*, E_{edge\pm\Delta})$ per stable specimen, where $E_{edge}$ represents the x-ray energy corresponding to the terbium $L_{III}$ absorption edge (7506 eV), and $\Delta = \pm 100$ eV. For the time-resolved, nonresonance x-ray diffraction study, only the edge-energy lamellar intensity functions $I_c(z^*, E_{edge})$ were analyzed further to derive the relative electron density profile for the multilayer unit cell containing two apposed profiles of the SR membrane, and the nonresonant changes in the unit cell and single SR membrane profile upon flash photolysis of caged ATP and subsequent protein phosphorylation in the multilayer specimens were determined (Asturias et al., 1994).

The time-resolved, resonance x-ray diffraction study involved the analysis of the background scattering-corrected, lamellar intensity functions as a function of x-ray energy at, versus off, the terbium $L_{III}$ absorption edge. First, the resonance effect was identified by calculating the direct arithmetic differences between lamellar intensity functions corresponding to different x-ray energy pairs, for data collected either before or after flash photolysis of caged ATP and subsequent protein phosphorylation in the stable SR multilayer specimens [i.e., $I_c^{res}(z^*, \Delta E)_E$ and $I_c^{res}(z^*, \Delta E)_{E\sim P}$].

The resonant contribution to the structure factor modulus for the multilayer electron density profile, before and after flash-photolysis of caged ATP ($|F_{ml}^{res}(z^*)|_E$ and $|F_{ml}^{res}(z^*)|_{E\sim P}$, was calculated directly from the appropriate corrected lamellar intensity functions, according to the following equation,

$$\begin{aligned} |F_{ml}^{res}(z^*)|^2 &= |F_{ml}(z^*, E_{edge}) - F_{ml}(z^*, E_{edge+\Delta})|^2 \\ &= |I_c^{1/2}(z^*, E_{edge}) - I_c^{1/2}(z^*, E_{edge+\Delta})|^2, \end{aligned} \quad (1)$$

where $F_{ml}(z^*, E_{edge})$ and $F_{ml}(z^*, E_{edge+\Delta})$ represent the multilayer profile structure factors at the edge energy ($E_{edge}$) and an off-edge energy ($E_{edge+\Delta}$), $I_c(z^*, E_{edge})$, and $I_c(z^*, E_{edge+\Delta})$ represent the corresponding experimentally measured, corrected lamellar intensity functions, and assuming that the resonance phenomenon has only a small effect on the phase of the multilayer profile structure factor (Asturias and Blasie, 1991; Blasie and Stamatoff, 1981).

For the phosphorylated enzyme conformation, the result for the post-UV flash resonant contribution to the structure factor modulus for the multilayer electron density profile $|F_{ml}^{res}(z^*)|_{E\sim P}$ calculated according to Eq. 1 was checked in the following, independent manner. For a multilayer unit cell profile possessing a center of symmetry, if the number of resonant atoms is only a small fraction of the total number of atoms in the multilayer unit cell, the resonant effect in the lamellar intensity function $I_c^{res}(z^*, \Delta E)$ arises almost exclusively from the interference between the resonant atoms and the nonresonant atoms in the structure (Blasie and Stamatoff, 1981; Stamatoff et al., 1982), and one can therefore write (dropping the subscript "c" and the argument "$\Delta E$" on "$I$" for simplification),

$$I^{res}(z^*) \simeq 2F(z^*)\cdot F^{res}(z^*), \quad (2)$$

where $F(z^*)$ and $F^{res}(z^*)$ denote the nonresonant and resonant contributions, respectively, to the structure factor for the multilayer electron density profile (dropping the subscript "ml" on "$F$" for simplification). The *change* in the resonant contribution to the lamellar intensity function *upon protein phosphorylation* $\Delta I^{res}(z^*)$ can then be expressed as

$$\begin{aligned} \Delta I^{res}(z^*) &= \Delta[2F(z^*)\cdot F^{res}(z^*)] \\ &\cong 2F(z^*)\cdot\Delta F^{res}(z^*) + 2F^{res}(z^*)\cdot\Delta F(z^*). \end{aligned} \quad (3)$$

Then, for only a very small change in the resonant contribution to the lamellar intensity function observed upon protein phosphorylation (i.e., $\Delta I^{res}(z^*) \cong 0$), one has the following relationship,

$$\frac{\Delta F^{res}(z^*)}{F^{res}(z^*)} \cong -\frac{\Delta F(z^*)}{F(z^*)}, \quad (4)$$

where $\Delta$ represents the change in $F(z^*)$ and $F^{res}(z^*)$induced by protein phosphorylation. Equation 4 demonstrates that, for $\Delta I^{res}(z^*) \simeq 0$, the fractional change induced by protein phosphorylation in the resonant contribution to the structure factor for the multilayer electron density profile for any value of $z^*$, $[\Delta F^{res}(z^*)/F^{res}(z^*)]$ is equal to the negative of the fractional change observed in the nonresonant contribution to the structure factor for the same $z^*$ value, $[\Delta F(z^*)/F(z^*)]$. This method has the advantage that the changes in the nonresonant contribution to the structure factor for the multilayer electron density profile can be measured with substantially higher accuracy and, therefore, Eq. 4 was used to confirm the correctness of the post-flash resonant contribution to the structure factor, ($|F^{res}(z^*)|_{E\sim P}$), as calculated using Eq. 1.

The next step was the calculation of the electron density profile of the resonant atoms within the multilayer profile structure, which is given directly by the phased inverse Fourier transform of the resonant contribution to the structure factor modulus for the multilayer electron density profile

$$\rho_{ml}^{res}(z) = \int |F_{ml}^{res}(z)| \exp(i\phi_{ml}^{res}(z^*))\exp(-2\pi i z^* z)\, dz^*. \quad (5)$$

The resonance structure factor modulus data obtained via Eq. 1 were phased using the iterative box-refinement procedure, employed previously by us in cases for which the multilayer possesses a substantial degree of lattice disorder of the second kind (Asturias and Blasie, 1991; Stroud and Agard, 1979). Finally, the GFSDM (Schwartz et al., 1975) analysis was used to "deconvolute" $\rho_{ml}^{res}(z)$ and thereby obtain the unit cell electron density profile for the resonant atoms, $\rho_{uc}^{res}(z)$, before and after protein phosphorylation. These profiles were then fitted, via a "real space refinement" analysis, with step-function model profiles to facilitate their interpretation in terms of the SR membrane molecular components.

## RESULTS

### Observation of the resonance diffraction effect and calculation of $|F_{ml}^{res}(z^*)|$ for the unphosphorylated ($Tb_xE$) and phosphorylated ($Tb_xE\sim P$) enzyme conformations

Lamellar x-ray diffraction data from hydrated, oriented multilayer specimens of isolated SR membranes at 4°C, which satisfied the criteria for multilayer specimen stability

described previously (Asturias et al., 1994), were examined for the presence of an appropriate resonance diffraction effect. As in our previous resonance diffraction work on this system (Asturias and Blasie, 1991), the resonance effect was sufficiently large to be readily apparent in the arithmetic differences between pairs of uncorrected, lamellar intensity functions collected from stable specimens at different x-ray energies in the vicinity of the lanthanide's $L_{III}$ absorption edge. This was the case for such differences calculated for data collected both before and after protein phosphorylation in the multilayer sample. A typical uncorrected lamellar intensity function $I_0(z^*, E)$, corresponding to a $Tb^{3+}$/$Ca^{2+}$ATPase mole ratio $\cong$4 and collected at 7606 eV (100 eV above the terbium $L_{III}$ absorption edge), and a corresponding difference intensity function $I^{res}(z^*, \Delta E_{ij})$ for $E_i$ = 7606 eV and $E_j$ = 7506 eV) from the same specimen before the flash photolysis of caged ATP and enzyme phosphorylation, are shown in Fig. 1 *A*. Fig. 1 *B* shows the resonant contribution to the structure factor modulus square for the multilayer electron density profile, calculated from the difference intensity function defined by Eq. 1. (Note that $I^{res}(z^*, \Delta E_{ij})$ and $|F^{res}_{ml}(z^*)|^2_E$ do *not* employ the same difference intensity function!] As can be seen from Fig. 1 *B*, the resonance diffraction data extend to $z^*_{max} = 0.025$ Å$^{-1}$, which corresponds to a spatial resolution of ~40 Å in the multilayer electron density profile. Comparison of the difference intensity function $I^{res}(z^*, \Delta E_{ij})$ shown in Fig. 1 *A* with such difference intensity functions from our previous lanthanide resonance x-ray diffraction work (Asturias and Blasie, 1991) indicates that the resonance effects on the lamellar diffraction for lanthanum and terbium are qualitatively similar (see Discussion) in nature for lanthanide/$Ca^{2+}$ATPase mole ratios of $\cong$4. In addition to using Eq. 1 to calculate directly the resonant contributions to the multilayer profile structure factor modulus for the unphosphorylated ($|F^{res}_{ml}(z^*)|_E$) and phosphorylated ($|F^{res}_{ml}(z^*)|_{E\sim P}$) enzyme conformations of the ATPase protein, the expression given in Eq. 4 was used to provide an independent corroboration of the results for ($|F^{res}_{ml}(z^*)|_{E\sim P}$) obtained using Eq. 1. The GFSDM analysis was used to calculate the nonresonant contribution to the structure factor modulus for the unit cell profile before ($|F_{uc}(z^*)|_E$) and after ($|F_{uc}(z^*)|_{E\sim P}$) enzyme phosphorylation. This result provided the fractional change $[\Delta F^{res}_{uc}(z^*)/F^{res}_{uc}(z^*)]$ via application of Eq. 4, which was then combined with the resonant unit cell profile structure factor modulus for the unphosphorylated enzyme conformation $|F^{res}_{uc}(z^*)|_E$, calculated according to Eq. 1, to provide the resonant contribution to the unit cell profile structure factor modulus after enzyme phosphorylation, $|F^{res}_{uc}(z^*)|_{E\sim P}$. (Note that for these oriented SR membrane multilayers possessing a relatively large degree of lattice disorder of the so-called second kind, the conversion of the resonant (or nonresonant) structure factor modulus for the multilayer profile to that for the unit cell profile is simply and unambiguously the Fourier transform of the appropriate generalized Patterson function, namely $Q^{res}_{ml}(z)$ in this case, over the multilayer unit cell 0 Å < $z$ < $D$, where $Q^{res}_{ml}(z)$ is just the inverse Fourier transform of $|F^{res}_{ml}(z^*)|^2_E$ and $D$ is the multilayer lattice periodicity.) Fig. 2 shows that there is very good agreement between the resonant contribution to the unit cell profile structure factor modulus for the phosphorylated enzyme conformation calculated directly from the post-UV flash resonance data using Eq. 1 (*dotted line*), or indirectly from the pre-UV flash resonant structure factor modulus $|F^{res}_{uc}(z^*)|_E$, and the fractional change in the nonresonant structure factor modulus $\Delta F_{uc}(z^*)/F_{uc}(z^*)$ observed upon enzyme phosphorylation using Eq. 4 (*dashed line*). Thus, two major changes are seen to occur in the resonant contribution to the structure factor modulus for the unit cell profile upon enzyme phosphorylation: the first maximum ($z^*$ < 0.005 Å$^{-1}$) nearly doubles in amplitude, and the second and third maxima ($z^*$ > 0.005 Å$^{-1}$) shift toward each other.

## Calculation of $\rho^{res}_{uc}(z)$ for the unphosphorylated and phosphorylated ATPase conformations

The resonant metal atom electron density profiles for the multilayer unit cell containing the apposed pair of SR single membrane profiles were derived for both the unphosphorylated ($Tb_xE$) and phosphorylated ($Tb_xE\sim P$) enzyme conformations, by calculating the phased Fourier transform of the appropriate resonant structure factor modulus for the multilayer profile (Eq. 5) over the interval $-D < z < +D$. The phases were determined using the so-called box-refinement algorithm (Stroud and Agard, 1979), an iterative refinement procedure that results in a unique solution for a centrosymmetric unit cell electron density profile, making no assumptions about the phases while maintaining a finite extent to the profile structure; we have shown that the latter constraint is appropriate for multilayers possessing a large degree of lattice disorder and that this algorithm provides the same solution as the GSFDM procedure, which assumes centrosymmetric phases (see Asturias and Blasie (1991) for greater detail). The so-calculated resonant metal atom electron density profiles for both forms of the enzyme are shown in Fig. 3. Examination of these metal electron density profiles at the low resolution of ~40 Å indicates that, upon phosphorylation of the ATPase, the metal density within the enzyme "headpiece" (*a*) and "stalk" (*b*) regions of the membrane profile is reduced, whereas the metal density within the lipid bilayer (*c*) and the intravesicular surface (*d*) regions of the membrane profile is increased.

## Modeling of the resonant metal atom unit cell electron density profiles $\rho^{res}_{uc}(z)$

Step-function electron density model profiles were refined, employing a real-space refinement analysis with phase information, to fit the continuous, resonant metal atom unit cell electron density profiles $\rho^{res}_{uc}(z)$, to facilitate their interpretation (Asturias and Blasie, 1991; Asturias et al., 1994). The general criteria used for the selection and testing of the step-function model profiles have been described previously (Asturias and Blasie, 1991; Asturias et al., 1994) and will not be presented here except for the two

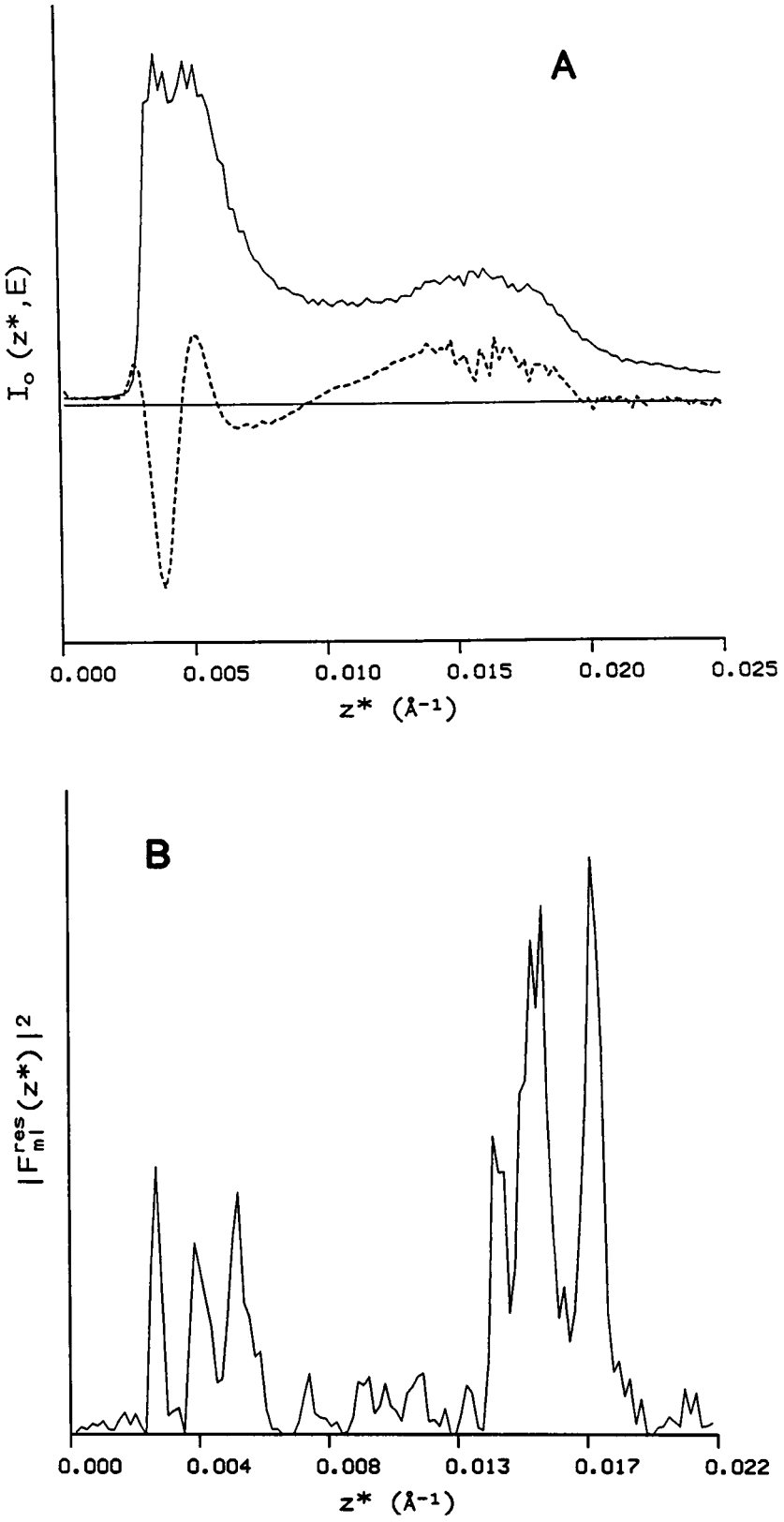


FIGURE 1 (*A*) Uncorrected lamellar intensity function $I_0(z^*, E)$ (———) collected at an x-ray energy of $E = [(Tb\,L_{IIIedge} + 100\text{ eV}) = 7606\text{ eV}]$ from a typical hydrated, oriented multilayer specimen of isolated SR membranes before the flash photolysis of caged ATP and enzyme phosphorylation, for a $Tb^{3+}/Ca^{2+}$ATPase mole ratio ~4, and the corresponding difference lamellar intensity function $I^{res}(z^*, \Delta E_{ij})$ (- - - - -), where $E_i = 7606$ eV and $E_j = 7506$ eV (see text for details). (*B*) Structure factor modulus square for the multilayer electron density profile of the resonant metal atoms $|F^{res}_{ml}(z^*)|^2_E$, calculated from the x-ray energy dependence of the lamellar intensity functions according to Eq. 1 (see text for details). The resonance diffraction data extend to $z^*_{max} = 0.025$ Å$^{-1}$, which corresponds to a spatial resolution of ~40 Å in the derived electron density profiles for the resonant metal atoms.

most important considerations, namely: a) the metal-binding sites were assumed to be discrete and localized in the membrane profile and, therefore, modeled as relatively thin (5 Å wide) electron density steps; and (b) the number of such discrete binding sites was constrained to the minimum required to account for the low-resolution resonance x-ray diffraction data. Given the relatively small magnitude of the changes in the continuous, resonant metal atom profile induced by enzyme phosphorylation and the resulting need to minimize any additional uncertainty introduced by the step-function model refinement, we chose to develop first a good step-function model profile for the continuous, resonant metal atom electron density profile corre-

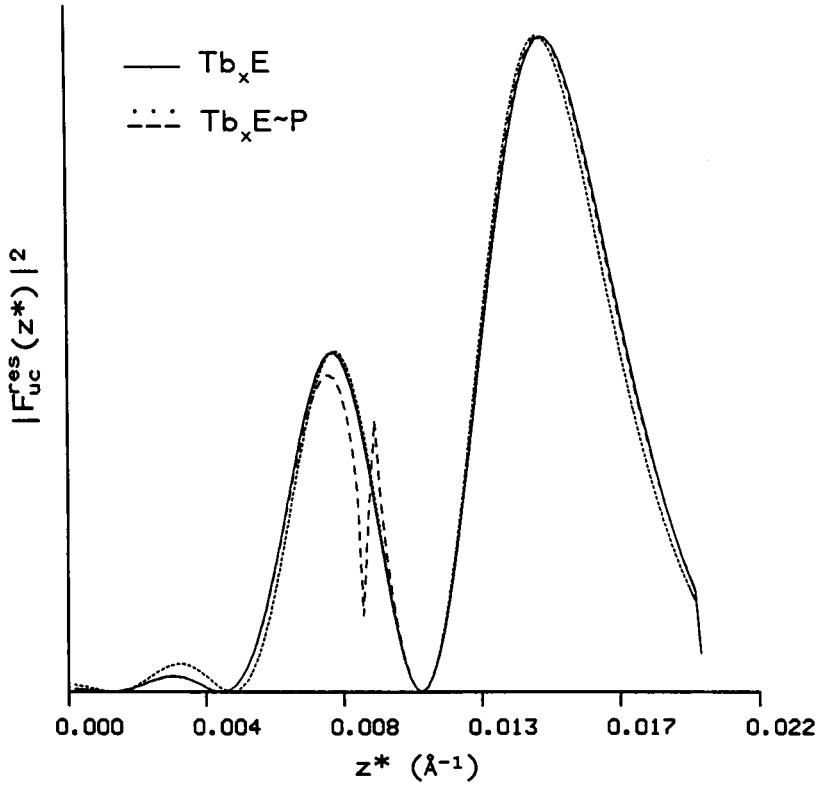


FIGURE 2 Resonant metal atom contribution to the structure factor modulus square $|F_{uc}^{res}(z^*)|^2$ for the multilayer unit cell electron density profile, before phosphorylation of the $Ca^{2+}$ATPase protein (———), and after enzyme phosphorylation (····· and – – –). $|F_{uc}^{res}(z^*)|^2_{E\sim P}$ for the phosphorylated enzyme conformation was calculated directly (·····) from the corresponding pre- and post-UV flash structure factor moduli for the resonant metal atom contributions to the multilayer electron density profile according to Eq. 1 (see text for details), or indirectly (- - -) according to Eq. 4 utilizing the pre-UV flash $|F_{uc}^{res}(z^*)|^2_E$ and the phosphorylation-induced fractional change in the nonresonant contribution to the structure factor modulus for the multilayer unit cell electron density profile. The discontinuity in the dashed line is due to the $z^*$-position of a zero in the nonresonant contribution to the unit cell structure factor modulus. See text for details.

sponding to the unphosphorylated enzyme conformation ($Tb_xE$). We then chose to search for those changes in this step-function resonant metal atom model profile, which would result in changes in the test functions employed in the real-space refinement that were consistent with the experimentally observed changes induced by protein phosphorylation (this matter is considered more carefully in the Discussion).

Fig. 4 *A* shows the refined step-function model profile for the continuous, resonant metal atom electron-density profile corresponding to the unphosphorylated enzyme conformation ($Tb_xE$), along with the continuous electron density profile for the asymmetric SR membrane contained within each half of the multilayer unit cell profile (the latter derived from the nonresonance lamellar x-ray diffraction data). The test functions employed in the real-space refinement analysis are shown in Fig. 4, *B* and *C*; they are: (a) the continuous, resonant metal atom unit cell electron density profile $\rho_{uc}^{res}(z)$, corresponding to the step-function model profile (calculated via double Fourier transformation including truncation of the structure factor for the step-function model profile to match the resolution of the experimental data), and (b) the resonant, unit cell structure factor modulus square $|F_{uc}^{res}(z^*)|^2_E$ [residual[2] $R_F = 7.03 \times 10^{-3}$]. Note that this modeling of the continuous, resonant metal atom unit cell electron density profile required a minimum of three localized metal-binding sites per single membrane. These sites are centered at $z = 2.5 \pm 2$, $35 \pm 2$, and $63 \pm 2$ Å. The locations of these localized metal-binding/transport sites in the membrane profile can be identified by referring to the electron density profile for the SR membrane, calculated from the nonresonance lamellar x-ray diffraction data at an intermediate resolution of ~15 Å (Asturias et al., 1994). The locations of these sites correspond to regions of the membrane profile containing (a) the phospholipid head groups of the inner phospholipid monolayer and the $Ca^{2+}$ATPase protein surface facing the intravesicular water space at $z = 2.5$ Å (20% of total metal density), (b) the "transbilayer" portion of the ATPase located approximately at the center of the membrane phospholipid bilayer at $z = 35$ Å (20% of total metal density), and (c) the junction of the "stalk" and "headpiece" portions of the $Ca^{2+}$ATPase at $z = 63$ Å (60% of total metal density). This is in contrast with the results from our lanthanum resonance x-ray diffraction studies (Asturias and Blasie, 1991), in which just two sites (a and c) proved sufficient to model successfully the lanthanum resonant metal atom profile. The origin and significance of this difference is discussed in the following section. Fig. 5 *A* shows the step-function model profile that best mimics the experimentally observed, enzyme phosphorylation-induced changes in the continuous, resonant metal atom unit cell electron density profile $\rho_{uc}^{res}(z)$ (Fig. 5 *B* as compared with Fig. 3), and the resonant metal atom unit cell structure factor modulus $|F_{uc}^{res}(z^*)|^2$ (Fig. 5 *C* as compared with Fig. 2). Note that the comparisons indicated above demonstrate that the changes to the step-function electron density model profile for the resonant metal atoms required to mimic the

[2] The residuals for a given function $f(x)_{calc}$ were calculated as

$$R_f = \Sigma [f(x)_{calc} - f(x)_{exp}]^2 / \Sigma [f(x)_{exp}]^2.$$

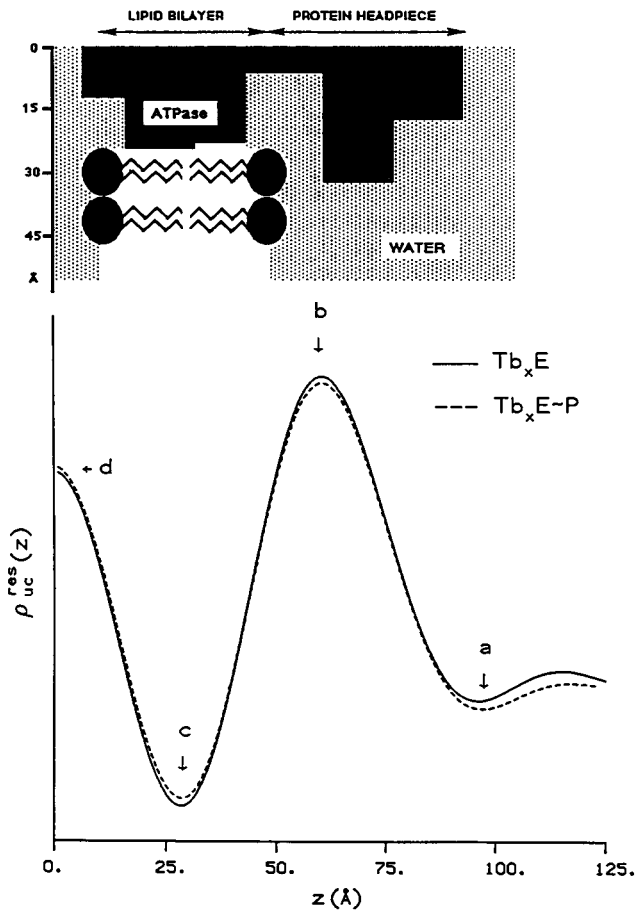


FIGURE 3 GFSDM-calculated resonant metal atom electron density profiles, for the SR membrane contained within each half of the multilayer unit cell profile, corresponding to the unphosphorylated ($Tb_xE$), and phosphorylated ($Tb_xE$~P) conformations of the $Ca^{2+}$ATPase. Examination of these low-resolution, resonant metal atom electron density profiles indicates that, upon phosphorylation of the ATPase, metal density is reduced within the enzyme "headpiece" (*a*) and "stalk" (*b*) regions of the SR membrane profile, and metal density is increased within the phospholipid bilayer (*c*) and the intravesicular surface (*d*) regions of the membrane profile. A schematic representation of the SR membrane profile to scale is included for reference.

major, experimentally observed effects of enzyme phosphorylation on $|F^{res}_{uc}(z^*)|^2$ are fully consistent with the changes observed in the experimentally derived, continuous resonant metal atom electron density profile; these changes include a decrease in the metal density for the "headpiece/stalk" site at $z = 63 \pm 2$ Å (namely, a 1% decrease in the metal density at this highly occupied site), and increases in the metal density for the phospholipid "bilayer center" site at $z = 35 \pm 2$ Å (namely, a 6% increase in the metal density at this lower occupancy site) and the "intravesicular surface" site at $z = 2.5 \pm 2$ Å (namely, a 3% increase in the metal density at this lower occupancy site).

## DISCUSSION

The terbium resonance x-ray diffraction studies described in the present paper were performed to determine possible changes in the occupancy and/or location of discrete metal-binding/transport sites in the $Ca^{2+}$ATPase profile structure within the SR membrane profile upon terbium-activated phosphorylation of the enzyme ($Tb_xE \rightarrow Tb_xE \sim P$). Direct measurements of terbium-activated enzyme phosphorylation and phosphoenzyme lifetime were used as the basis for the design of both the time-resolved, nonresonance and time-resolved, resonance x-ray diffraction experiments. The time-resolved, nonresonance x-ray diffraction measurements (described in the accompanying paper (Asturias et al., 1994)) indicated that significant changes occur in the profile structure of the SR membrane upon terbium-activated phosphorylation of the ATPase enzyme. These "large-scale" (i.e., long-range) changes in the low-resolution electron density profile of the membrane were qualitatively similar in nature, but smaller in magnitude, as compared with the changes in the membrane profile structure observed upon calcium-activated enzyme phosphorylation. On the other hand, the time-resolved, resonance x-ray diffraction experiments described here were exclusively sensitive to the distribution of the terbium atoms present in the membrane profile and provided information concerning the changes in the distribution of these metal atoms upon enzyme phosphorylation. In this section, the nature and significance of the results from the time-resolved, resonance x-ray diffraction study are discussed and correlated with the results from the time-resolved, nonresonance x-ray diffraction work, as well as with the results from independent, time-resolved x-ray diffraction studies of calcium binding to the ATPase (DeLong and Blasie, 1993).

### Calculation of $|F^{res}_{uc}(z^*)|^2$ and $\rho^{res}_{uc}(z)$ for the unphosphorylated ($Tb_xE$) and phosphorylated ($Tb_xE \sim P$) enzyme conformations

The resonant metal atom structure factor moduli for the multilayer unit cell profile $|F^{res}_{uc}(z^*)|^2$ for the unphosphorylated and phosphorylated enzyme conformations were calculated directly according to Eq. 1, noting the simple and unambiguous conversion of a structure factor modulus for the multilayer profile to that for the unit cell profile for multilayers possessing a sufficient degree of lattice disorder of the so-called second kind (see Figs. 1 *B* and 2). However, examination of the resonance x-ray diffraction data indicated that the changes observed in the difference intensity functions $I^{res}(z^*, \Delta E_{ij})$ upon enzyme phosphorylation were relatively small, and this observation led to our consideration of the expression in Eq. 4, which provided an independent method for calculating the resonant contribution to the unit cell structure factor modulus square $|F^{res}_{ml}(z^*)|^2$ after enzyme phosphorylation. By using Eq. 1, the resonant contribution to the unit cell structure factor modulus square $|F^{res}_{uc}(z^*)|^2$ for the unphosphorylated and phosphorylated enzyme conformations were calculated independently of each other, and the phosphorylation-induced change in the resonant contribution to this structure factor modulus was calculated by taking the difference between these two functions. Use of Eq. 4, how-

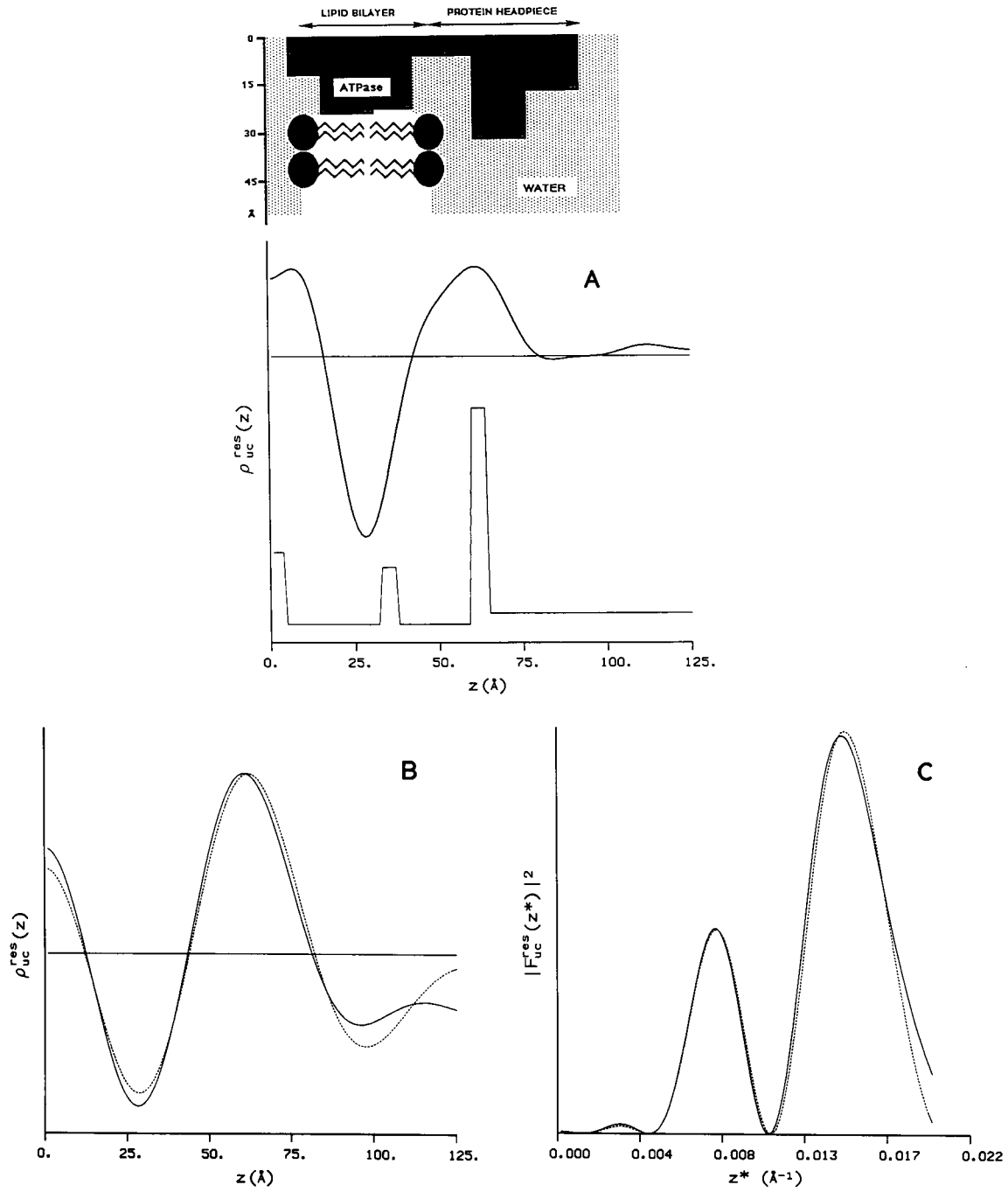


FIGURE 4 Modeling of the low-resolution, resonant metal atom unit cell electron density profile $\rho_{uc}^{res}(z)$ for the unphosphorylated ($Tb_xE$) enzyme conformation. The best step-function electron density model profile has three discrete, localized metal binding sites per single membrane profile, modeled by 5-Å-wide steps centered at $z = 2.5 \pm 2$, $35 \pm 2$, and $63 \pm 2$ Å. (*A*) Refined best step-function model profile. The unit cell electron density profile of the SR membrane, as well as a schematic representation of the membrane profile structure to scale are included for reference. (*B*) Experimental, resonant metal atom unit cell electron density profile $\rho_{uc}^{res}(z)_E$ (———) and the continuous electron density profile (·····, calculated via double Fourier transformation at 40-Å resolution) corresponding to the refined, best step-function model profile for the resonant metal atoms. (*C*) Experimental (———) and refined, best step-function model (·····) resonant contributions to the unit cell structure factor modulus $|F_{uc}^{res}(z^*)|_E^2$ (residual $R_F = 7.03 \times 10^{-3}$).

ever, allows the calculation of the *change* in the resonant contribution to the structure factor modulus directly in terms of the resonant contribution to the structure factor modulus before enzyme phosphorylation and the phosphorylation-induced fractional change in the nonresonant structure factor modulus. Furthermore, because the resonance diffraction effect is usually less than a few percent of the lamellar intensity function for such dilute resonant metal atom concentrations in these membrane multilayers, the utilization of the much more precisely determined nonresonant contribution to the structure factor modulus offers a significant advantage. Nevertheless, the changes in the resonant contribution to the

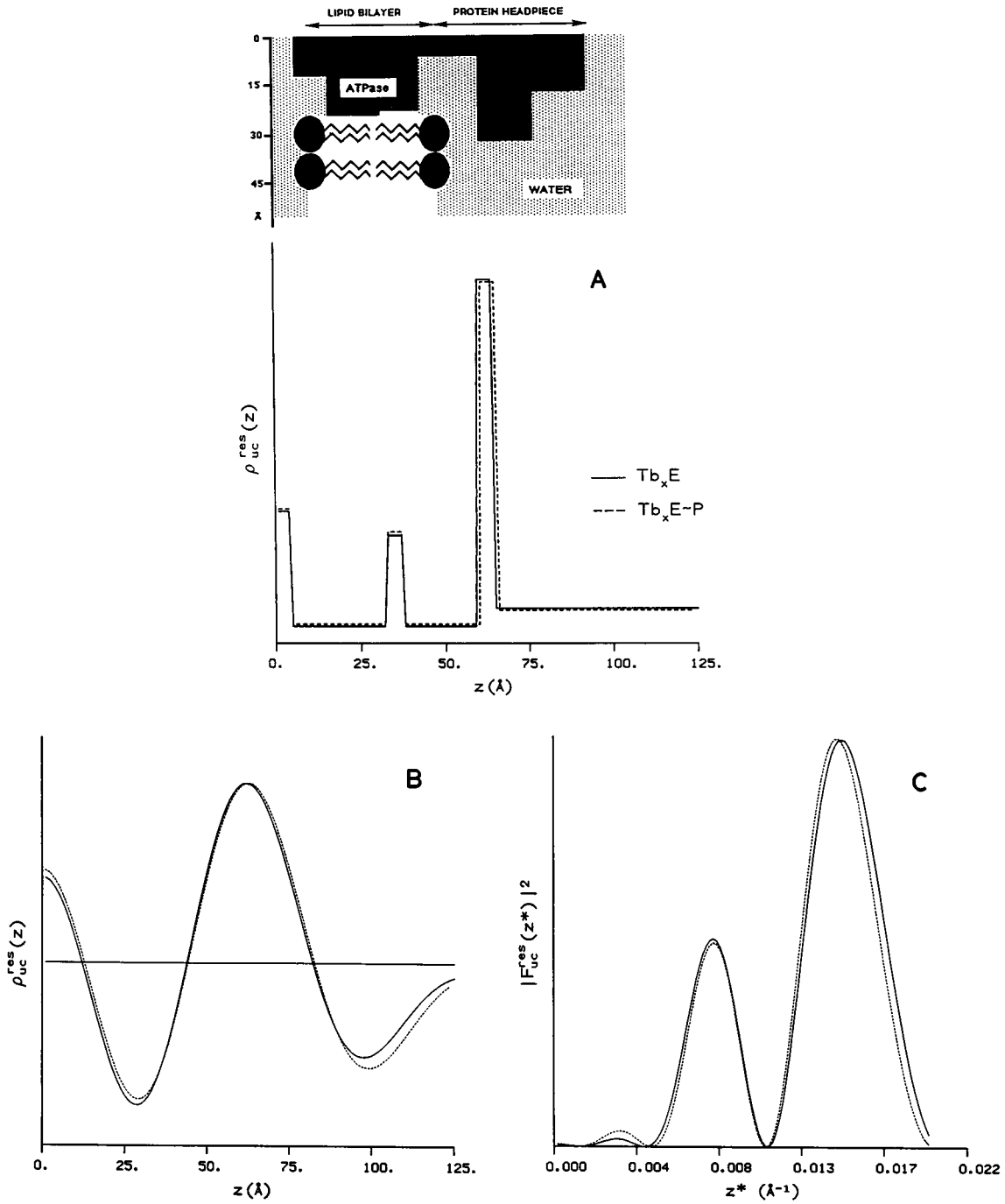


FIGURE 5 Modeling of the changes in the resonant metal atom unit cell electron density profile $\rho^{res}_{uc}(z)$ induced by enzyme phosphorylation. The refined, best step-function model corresponding to the unphosphorylated conformation of the ATPase was used as the starting point, and was modified to mimic the phosphorylation-induced changes in the experimentally derived "test" functions of *B* and *C* below. (*A*) Refined, best resonant metal atom step-function model profiles for the unphosphorylated ($Tb_xE$, ———) and phosphorylated ($Tb_xE$~P) enzyme conformations. (*B*) Continuous electron density profiles (calculated via double Fourier transformation at 40-Å resolution) corresponding to the refined, best step-function model profiles for the resonant metal atom unit cell electron density profiles $\rho^{res}_{uc}(z)$, for the unphosphorylated (———) and phosphorylated enzyme conformations (to be compared with their experimentally derived counterparts in Fig. 3). (*C*) Unit cell structure factor modulus square $|F^{res}_{uc}(z^*)|^2$ for the refined, best resonant metal atom step-function model profiles for the unphosphorylated (———) and phosphorylated enzyme conformations (to be compared with their experimentally derived counterparts in Fig. 2).

structure factor modulus for the multilayer unit cell profile induced by enzyme phosphorylation, as determined by these two independent approaches, are essentially identical (see Fig. 2), and the changes are significant. Enzyme phosphorylation induces a very large change in the amplitude of the first low-$z^*$ maximum (nearly 100%), and the centroids of the second and third maxima at higher-$z^*$ shift significantly toward each other; the latter feature is relatively insensitive to the counting-statistics noise for the individual $z^*$-values in the experimental data, but is very sensitive to small changes

in the distribution of metal density in the unit cell and single membrane profiles. Having thereby reliably determined the resonant contribution to the structure factor modulus for the unit cell profile for both the unphosphorylated and phosphorylated enzyme conformations, we then proceeded with the analysis of these data to obtain the resonant metal atom electron density profiles $\rho_{uc}^{res}(z)$ shown in Fig. 3.

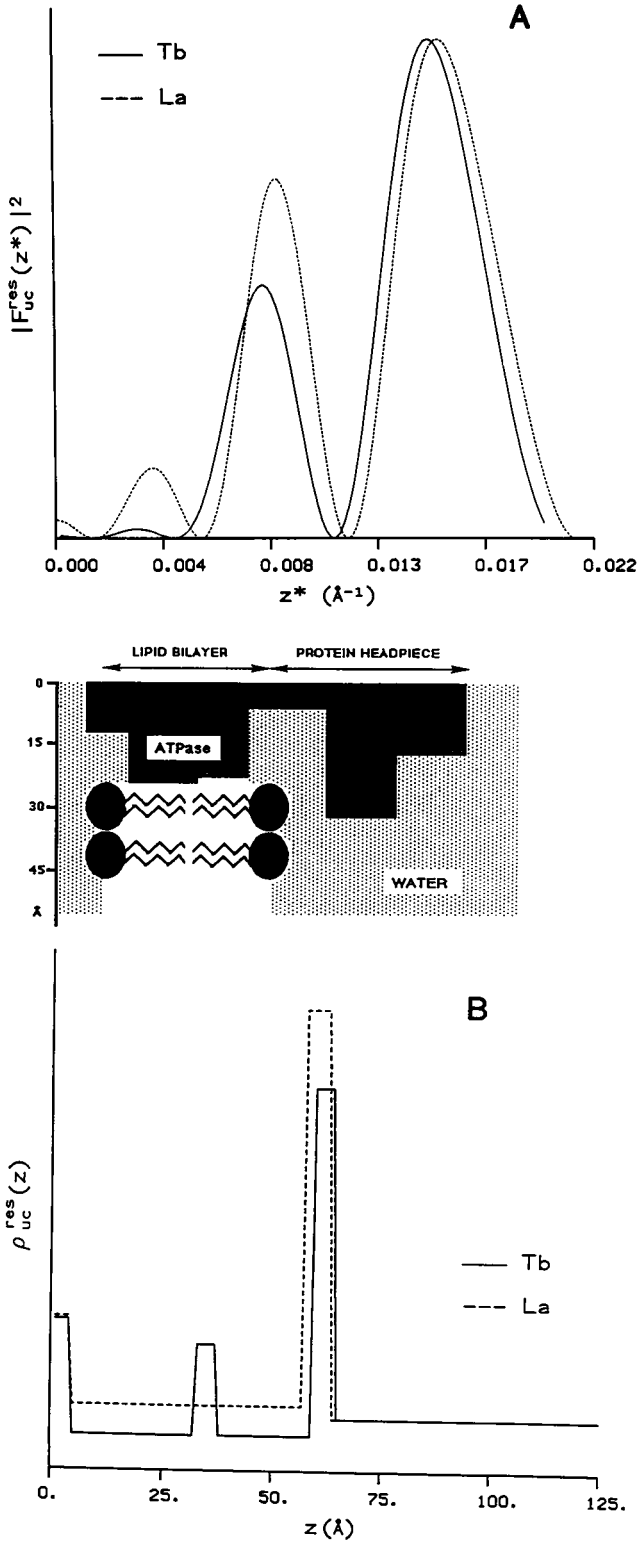


## $\rho_{uc}^{res}(z)$ for the unphosphorylated enzyme conformation: comparison between the lanthanum and terbium metal electron density profiles

Identification of the terbium resonance x-ray diffraction effect in the $I^{res}(z^*, \Delta E_{ij})$ data for these experiments was facilitated by its qualitative similarity to the lanthanum resonance diffraction effect described in our previous study of the profile structure of the SR $Ca^{2+}$ATPase (Asturias and Blasie, 1991). Nevertheless, close examination of the data revealed the existence of very significant differences between the terbium and lanthanum resonance effects. This was more readily apparent upon comparison of the resonant contributions to the unit cell structure factor modulus squared $|F_{uc}^{res}(z^*)|^2$, derived as described for each lanthanide. As can be seen from Fig. 6 *A*, these $|F_{uc}^{res}(z^*)|^2$ functions are qualitatively similar only in that they contain the same number of maxima over a comparable range of $z^*$, and the relative amplitudes of the maxima increase with increasing $z^*$. These similarities might suggest, at least intuitively, that the distributions of lanthanum and terbium across the membrane profile contain some common features. However, the substantial differences in the relative amplitudes of the first two maxima ($0.002\ Å^{-1} \leq z^* \leq 0.012\ Å^{-1}$) and the smaller, but significant differences in the $z^*$-positions of the centroids of the maxima are sufficient to cause a very significant difference in the distribution of the two lanthanides in the membrane profile, as compared in their step-function model profiles shown in Fig. 6 *B*.

Only two localized metal sites were necessary to model completely the low-resolution, resonant lanthanum atom profile in the real-space refinement analysis. Addition of a third site could not produce any significant improvement in the fits of the model functions to their experimental counterparts in this analysis. However, we did tentatively include a third site (Asturias and Blasie, 1991), located in the region of the membrane profile corresponding to the phospholipid headgroups at the extravesicular membrane surface, which produced only a marginal improvement in the model. Inclusion of this third site was motivated by our interest in gaining some additional insight concerning the nature of one of the two significant binding sites located in the region of the profile corresponding to the phospholipid polar head-

FIGURE 6 Comparison between the lanthanum and terbium resonant metal atom electron density profiles derived from the resonance x-ray diffraction experiments. (*A*) Resonant contribution to the unit cell structure factor modulus square $|F_{uc}^{res}(z^*)|_E^2$ for terbium (———) and lanthanum. Note that although both functions contain the same number of maxima over this range of $z^*$, the relative amplitudes and positions of those maxima are significantly different for the two lanthanides. (*B*) Refined, best step-function resonant metal atom electron density profiles for terbium (———) and lanthanum reflecting the differences in their respective unit cell structure factor modulus squares. Two localized metal binding sites (centered at $z$ = 2.5 and 61 Å) are sufficient to model completely the lanthanum profile. Modeling of the terbium profile requires an additional site (centered at $z$ = 35 Å), located in the phospholipid bilayer region of the membrane profile. See text for a discussion of this result.

groups and the ATPase protein located at the intravesicular surface of the membrane profile at $z = 2.5 \pm 2$ Å. We expected that, if lanthanum was binding to the phospholipid headgroups at the intravesicular surface, some binding to the phospholipid headgroups at the extravesicular surface would also occur. The only marginal improvement produced by the addition of this third lowest occupancy site located in the region of the membrane profile containing the extravesicular phospholipid headgroups suggested that the significant site at $z = 2.5 \pm 2$ Å was most likely a site on the ATPase protein.

Initially, we tried to model the low-resolution, terbium resonant atom profile using only the two localized metal-binding sites that were sufficient to model completely the lanthanum resonant atom profile, but then found that an additional metal-binding site was absolutely necessary to provide a satisfactory model of the terbium profile via the real-space refinement analysis. Examination of the low-resolution, experimental unit cell electron density profiles for the resonant terbium atoms shown in Fig. 3 suggested placing the third metal-binding site in the region of the membrane profile containing the phospholipid bilayer and the "transbilayer" portion of the $Ca^{2+}$ATPase, because a significant increase in metal density is observed in that region upon phosphorylation of the ATPase protein. The assumption of a finite number of discrete, localized metal-binding sites (as justified in detail in Asturias and Blasie (1991)) within a single SR membrane profile, and the presence of two apposed single membrane profiles within the multilayer unit cell profile causes the functions employed to test the adequacy of the model resonant atom profile in the real-space refinement analysis to be extremely sensitive to the positions of these sites, even when utilizing relatively low-resolution resonance x-ray diffraction data. As a result, it is possible to determine the positions of the discrete metal-binding sites to a precision much greater than the resolution of the continuous, low-resolution unit cell electron density profiles for the resonant metal atoms. As can be seen in Fig. 5 *A*, the additional metal-binding site centered at $z = 35 \pm 2$ Å is located near the center of the phospholipid bilayer region of the membrane profile.

In designing these resonance x-ray diffraction experiments, we purposely chose to use terbium as the lanthanide analog for $Ca^{2+}$, because it had been reported that the capacity of terbium to displace $Ca^{2+}$ from the high-affinity metal binding/transport sites on the ATPase was roughly an order of magnitude higher than that of lanthanum (Squirer et al., 1990) (for more details see Asturias et al., 1994). The fact that the "transbilayer" site on the enzyme centered at $z \cong 35$ Å was occupied by terbium, but not lanthanum at lanthanide/$Ca^{2+}$ATPase mole ratios of $\cong 4$ suggests that this particular site has the highest binding affinity for calcium, because it was more difficult to displace calcium from it as opposed to the "stalk"/"headpiece" and "intravesicular surface" sites similarly occupied by both lanthanides. These three distinct metal-binding sites identified in the SR membrane profile by the terbium resonance x-ray diffraction studies, represent the minimum number of discrete sites necessary to account for the experimentally derived, low-resolution resonant metal atom electron density profile. Extension of the resonance x-ray diffraction work to higher resolution could indicate the existence of additional sites in the membrane profile. However, any such new sites would be expected to lie within the narrow regions defined by the uncertainty in the positions ($\pm 2$ Å) of these three sites already identified in this low-resolution study.

## Interpretation of the terbium metal electron density profiles: significance of the changes observed upon protein phosphorylation

The conditions for the present experiments were chosen to maximize the displacement of $Ca^{2+}$ from and the binding of $Tb^{3+}$ to the high-affinity metal-binding/transport sites on the SR ATPase protein, while simultaneously minimizing the amount of nonspecific terbium binding, including binding to the membrane phospholipids (Asturias et al., 1994). Measurements of the enzyme phosphorylation level and the phosphoenzyme lifetime indicated that, under the conditions of our experiments, terbium itself can activate phosphorylation of the ATPase (Asturias et al., 1994). Analysis of the time-resolved, nonresonance x-ray diffraction data (Asturias et al., 1994) confirmed the results obtained from the enzyme phosphorylation measurements by detecting significant changes in the profile structure of the SR membrane upon flash photolysis of caged ATP, and subsequent enzyme phosphorylation in the multilayer specimens used for the x-ray diffraction work (Asturias et al., 1994). The "large-scale" (i.e., long-range) changes in the membrane profile upon terbium-activated phosphorylation of the ATPase protein were found to be qualitatively similar in nature to those observed upon calcium-activated phosphorylation (Asturias et al., 1994), a result that substantiated the "physiological" relevance of undertaking a time-resolved, terbium resonance x-ray diffraction study of this SR membrane system.

The most immediate conclusion derived from the results of the terbium resonance x-ray diffraction experiments is that a finite number (at least three) of discrete, localized metal-binding/transport sites exist spanning most of the SR membrane profile, all of which are simultaneously occupied to an extent that reflects their individual binding affinities (at equilibrium). This observation is in agreement with the results from our previous lanthanum resonance x-ray diffraction work (Asturias and Blasie, 1991). We believe that all three of the sites identified are sites on the ATPase protein, including the site located at the intravesicular surface of the membrane ($z = 2.5 \pm 2$ Å), for the reasons described above. The positions of these metal-binding/transport sites in the profile of the membrane do not change significantly upon phosphorylation of the ATPase protein. Instead, a small but significant redistribution of metal density among these sites occurs upon enzyme phosphorylation. This nature of these enzyme phosphorylation-induced changes (namely, a net inward shift of metal density toward the intravesicular membrane surface) strongly suggests that these sites play an active

role in the translocation of ions across the SR membrane profile, the redistribution of metal density being a direct result of the "large-scale" (i.e., long-range) structural changes that occur in the profile structure of the ATPase upon its phosphorylation. In modeling the changes in the metal density distribution induced by enzyme phosphorylation, the model resonant metal atom profile for the resting enzyme conformation $Tb_xE$, was changed in a way that conserved the total resonant metal atom electron density. This can be readily appreciated if the percentage change in the occupancy of each of the three metal binding sites stated in Results are applied to the magnitude of the electron density step used to best model each individual site. The small number (three) of discrete, localized metal binding/transport sites required to completely model the resonant metal atom profile for the $Tb_xE$ unphosphorylated form of the enzyme presented a major constraint upon attempting to model the resonant metal atom profile for the phosphorylated $Tb_xE\sim P$ form *only* in terms of changes (position and/or occupancy) in the three sites for $Tb_xE$ form; in fact, the result achieved via the real-space refinement analysis for the phosphorylated $Tb_xE\sim P$ form is unique given this constraint. We estimate the uncertainty in the magnitude of the changes in the individual steps in the step-function model profiles to be between 0.2 and 0.5%, depending on the amplitude of the step involved (the uncertainty being inversely proportional to the amplitude of the step). It is important to note that magnitude of the redistribution of metal density among the binding/transport sites induced by enzyme phosphorylation (expressed as percentage changes in the metal density at the different sites) should be corrected to account for the incomplete lanthanide-activated phosphorylation of the ATPase protein ensemble under the experimental conditions (Asturias et al., 1994). This results in an increase over the values stated in Results by a factor of 2 to 6.

Binding of terbium to these high-affinity binding/transport sites has a profound effect on the functionality of the SR membrane $Ca^{2+}$ATPase, as evidenced by the significant extension in the lifetime of the phosphorylated enzyme observed in the presence of terbium. As indicated in the accompanying paper (Asturias et al., 1994), we believe that this extension in the lifetime of the phosphorylated enzyme is not due, as has been proposed (Fujimori and Jencks, 1990), to the use of a lanthanide-ATP complex as the substrate for the enzyme. Under the conditions of our experiments, very little terbium should be available after the high-affinity metal-binding/transport sites on the ATPase have been occupied. This makes it unlikely that sufficient terbium would remain to compete effectively with magnesium for complexation with ATP and bind at the catalytic site (Asturias et al., 1994). Furthermore, the results from our lanthanum and terbium resonance x-ray diffraction studies show that no lanthanide-binding site is detected in the region of the membrane profile corresponding to the proposed location of the nucleotide binding site based on fluorescence energy transfer measurements (Bigelow and Inesi, 1991)—namely, on the portion of the ATPase "headpiece" that is 35–40 Å away from the extravesicular surface of the membrane phospholipid bilayer, near the edge of the unit cell profile. The only "stalk"/"headpiece" site identified by our lanthanide resonance x-ray diffraction experiments is located only 12 ± 2 Å from the extravesicular surface of the membrane phospholipid bilayer.

Independent evidence supporting our conclusion that the metal-binding/transport sites identified by our terbium resonance x-ray diffraction study are involved in active calcium transport is provided by the results from a separate, time-resolved x-ray diffraction study of calcium binding to the SR membrane (DeLong and Blasie, 1993). In that work, a calcium cage molecule (DM-nitrophen; Ellis-Davies and Kaplan, 1988) was used to synchronously release calcium in otherwise calcium-free, oriented SR membrane multilayer specimens, thereby allowing the study of the profile structure of the membrane for the transition from the calcium-free, unphosphorylated conformation of the enzyme to the calcium-bound, unphosphorylated conformation (i.e., $E \rightarrow Ca_xE$). The results from this study indicate that the changes observed in the SR membrane profile structure upon calcium binding are localized, and can be explained by the addition of calcium to three discrete binding sites in the membrane profile and small changes in the profile structure of the ATPase protein adjacent to these sites (DeLong and Blasie, 1993). These calcium binding sites occur in the membrane profile almost exactly at the positions of the terbium binding sites determined by our resonance x-ray diffraction work.

Finally, it is important to point out that the positions of the identified high-affinity metal-binding/transport sites within the SR membrane profile structure are in general agreement with the results from other studies, including potential metal-binding sites identified within the putative secondary/tertiary structure for the $Ca^{2+}$ATPase based on its primary sequence (MacLennan et al., 1985), fluorescence energy-transfer measurements (Squirer et al., 1990) indicating that the predominant lanthanide binding site is located in the "headpiece"/"stalk" portion of the enzyme structure, and studies of the effect of site-directed mutagenesis of selected amino acid residues located in a number of potential metal-binding sites within the putative three-dimensional structure of the $Ca^{2+}$ATPase on various aspects of the active calcium transport process (Clarke et al., 1989).

## CONCLUSIONS AND IMPLICATIONS FOR ACTIVE CALCIUM TRANSPORT

Three discrete, high-affinity metal-binding/transport sites have been identified in the SR membrane profile structure by our terbium resonance x-ray diffraction work. Phosphorylation of the $Ca^{2+}$ATPase protein results in a small, but significant, redistribution of metal density among those sites. The relatively small magnitude of this redistribution of terbium among these sites upon enzyme phosphorylation results mostly from incomplete lanthanide-activated phosphorylation of the ATPase protein ensemble, and also possibly from the inability of lanthanides to completely replace calcium as

the ion transported by the enzyme. The results from independent structural studies of calcium binding indicate that although lanthanides may not be perfect calcium analogs (as suggested by the fact that it seems to be difficult to measure significant net transport of lanthanides across the SR membrane), they seem to bind to the same sites within the SR membrane profile structure as calcium. Thus, we would expect that the redistribution of calcium among these metal-binding/transport sites within the SR membrane profile, induced by phosphorylation of the ATPase, to be analogous to but much larger than that observed for terbium. Indeed, the precise magnitude of the redistribution of terbium among the so-identified metal-binding/transport sites is not especially crucial for the general conclusions reached from the work described here.

Our time-resolved, nonresonance x-ray diffraction studies indicate that small, but significant, changes in the electron density profile of the SR membrane are induced by phosphorylation of the $Ca^{2+}$ATPase, activated by the binding of either calcium or terbium to the high-affinity metal-binding/transport sites on the enzyme. These small changes have been termed "large-scale" or long-range because they occur across the entire profile structure of the SR membrane, but they are much too small to represent shifts of large portions of protein mass from one specific region of the membrane profile to another (Blasie et al., 1985; Pascolini et al., 1988; Asturias et al., 1994; Blasie et al., 1990). Furthermore, the results from our time-resolved, resonance x-ray diffraction work indicate that for both the unphosphorylated ($Tb_xE$) and phosphorylated ($Tb_xE\sim P$) conformations of the ATPase protein, a small, finite number of discrete, high-affinity metal-binding/transport sites are distributed over most of the membrane profile structure, and they are all occupied simultaneously to varying extents depending on the phosphorylation state of the enzyme. A number of $\alpha$-helical polypeptide chain segments are proposed to span the lipid bilayer of the SR membrane composing the "transbilayer" and "stalk" portions of the putative three-dimensional structure of the $Ca^{2+}$ATPase (MacLennan et al., 1985), and they have also been identified by electron microscopic image-reconstruction studies of two-dimensionally crystalline forms of the ATPase (Stokes and Green, 1990). This bundle of $\alpha$ helices may form a "channel" across the SR membrane phospholipid bilayer (Inesi et al., 1992). Together, the above considerations support an "active channel" type of mechanism for active ion transport by the SR ATPase. Thus, the transport of ions across the membrane profile would be accomplished by redistributing ions among a finite number of discrete sites along this "active channel" spanning the membrane's phospholipid bilayer. A redistribution of ions among these sites would take place whenever the *relative* binding affinities of the different sites along the "active channel" were altered by small, local conformational changes in the ATPase protein at one or more of the sites. In this "active channel" mechanism, the "large-scale" or long-range changes in the profile structure of the enzyme induced by its phosphorylation, would cause the affinity of the sites along the channel to vary in a concerted manner that would result in net, vectorial transport of ions across the membrane. The enzyme phosphorylation-induced "large-scale" changes would represent changes in helix-helix interactions propagated along the $\alpha$-helical bundle and manifest as changes in the local area/helix (and, hence, protein electron density) within the various regions of the membrane profile. Finally, the most highly occupied sites located at the junction of the enzyme "stalk" and "headpiece" would arise due to the number, and not the relative binding-affinities, of metal-binding sites at this location in the enzyme's profile structure, the "transbilayer" site on the enzyme having the highest binding affinity. Thus, these sites at the "stalk"/"headpiece" junction could represent the extravesicular end of the "active channel," their higher number but lower affinities thereby facilitating the active transport process simply by increasing the local concentration of the metal ion to be transported at that end of the "active channel."

This work was supported by National Institutes of Health grants HL-18708 Project 2 and RR01633 to J. K. Blasie.

## REFERENCES

Asturias, F. J., and J. K. Blasie. 1991. Location of high-affinity metal binding sites in the profile structure of the $Ca^{2+}$ATPase in the sarcoplasmic reticulum by resonance x-ray diffraction. *Biophys. J.* 59:488–502.

Asturias, F. J., R. F. Fischetti, and J. K. Blasie. 1994. Changes in the profile structure of the sarcoplasmic reticulum membrane upon phosphorylation of the $Ca^{2+}$ATPase enzyme in the presence of terbium: a time resolved x-ray diffraction study. *Biophys. J.* 66:1653–1664.

Bigelow, D. J., and G. Inesi. 1991. Frequency-domain fluorescence spectroscopy resolves the location of maleimide-directed spectroscopic probes within the tertiary structure of the Ca-ATPase of sarcoplasmic reticulum. *Biochemistry.* 30:2113–2125.

Blasie, J. K., D. Pascolini, F. J. Asturias, L. Herbette, D. Pierce, and A. Scarpa. 1990. Large-scale structural changes in the sarcoplasmic reticulum ATPase appear essential for calcium transport. *Biophys. J.* 58:687–693.

Blasie, J. K., L. Herbette, D. Pascolini, V. Skita, D. Pierce, and A. Scarpa. 1985. Time-resolved x-ray diffraction studies of the sarcoplasmic reticulum membrane during active transport. *Biophys. J.* 48:9–18.

Blasie, J. K., and J. Stamatoff. 1981. Resonance x-ray scattering: its use in determining spatial relationships among metal atoms within macromolecules in a non-crystalline state. *Annu. Rev. Biophys. Bioeng.* 10:451–458.

Clarke, D., K. Maruyama, T. Loo, E. Leberer, G. Inesi, and D. MacLennan. 1989. Functional consequences of glutamate, aspartate, glutamine, and asparagine mutations in the stalk sector of the $Ca^{2+}$ATPase of sarcoplasmic reticulum. *J. Biol. Chem.* 264:11246–11251.

Clarke, D., T. Loo, G. Inesi, and D. MacLennan. 1989. Location of high affinity $Ca^{+2}$-binding sites within the predicted transmembrane domain of the sarcoplasmic reticulum $Ca^{+2}$ATPase. *Nature (Lond.).* 339: 476–478.

DeLong L., and J. K. Blasie. 1993. Effect of $Ca^{2+}$ binding on the profile structure of the sarcoplasmic reticulum membrane employing time-resolved x-ray diffraction. *Biophys. J.* 65:1750–1779.

Ellis-Davies, G. C., and J. H. Kaplan. 1988. Photolabile chelators for the rapid photorelease of divalent cations. *Proc. Natl. Acad. Sci. USA.* 85: 6571–6575.

Fujimori, T., and W. Jencks. 1990. Lanthanum inhibits steady-state turnover of the sarcoplasmic reticulum calcium ATPase by replacing magnesium as the catalytic ion. *J. Biol. Chem.* 265:16262–16270.

Herbette, L., P. DeFoor, S. Fleischer, D. Pascolini, A. Scarpa, and J. K. Blasie. 1985. The separate profile structures of the functional calcium pump protein and the phospholipid bilayer within isolated sarcoplasmic reticulum membranes determined by x-ray and neutron diffraction. *Biochim. Biophys. Acta.* 817:103–122.

Inesi, G. 1985. Mechanism of calcium transport. *Annu. Rev. Physiol.* 47: 573–601.

Inesi, G., D. Lewis, D. Nikic, A. Hussain, and M. E. Kirtley. 1992. Long-range intramolecular linked functions in the calcium transport ATPase. *Adv. Enzymol. Mol. Biol.* 65:185–215.

MacLennan, D. H., C. J. Brandl, B. Korczak, and N. M. Green. 1985. Amino Acid sequence of a $Ca^{+2}$ + $Mg^{+2}$-dependent ATPase from rabbit muscle sarcoplasmic reticulum, deduced from its complimentary DNA sequence. *Nature.* 316:696–700.

MacLennan, D. H., C. J. Brandl, B. Korczak, and N. M. Green. 1985. Amino-acid sequence of a $Ca^{2+}$ + $Mg^{2+}$-dependent ATPase from rabbit muscle sarcoplasmic reticulum, deduced from its complementary DNA sequence. *Nature.* 316:696–700.

Meissner, G., and S. Fleischer. 1974. Dissociation and reconstitution of functional sarcoplasmic reticulum vesicles. *J. Biol. Chem.* 249:302–309.

Pascolini, D., L. Herbette, V. Skita, F. J. Asturias, A. Scarpa, and J. K. Blasie. 1988. changes in the sarcoplasmic reticulum membrane profile induced by enzyme phosphorylation to $E_1$~P at 16 Å resolution via time-resolved x-ray diffraction. *Biophys. J.* 54:679–688.

Schwartz, S., J. Cain, E. Dratz, and J. K. Blasie. 1975. An analysis of lamellar x-ray diffraction from disordered membrane multilayers with application to data from retinal rod out segments. *Biophys. J.* 15: 1201–1233.

Squier, T., D. Bigelow, F. J. Fernandez-Belda, L. deMeis, and G. Inesi. 1990. Calcium and lanthanide binding in the sarcoplasmic reticulum ATPase. *J. Biol. Chem.* 265:13713–13720.

Stamatoff, J., P. Eisenberger, J. K. Blasie, J. Pachence, A. Tavormina, M. Erecinska, P. L. Dutton, and G. Brown. 1982. The location of redox centers in biological membranes determined by resonance x-ray diffraction. I. Observation of the resonance effect. *Biochim. Biophys. Acta.* 679: 177–187.

Stokes, D. L., and N. M. Green. 1990. A comparison of frozen-hydrated and negatively stained crystals of calcium ATPase suggest a shape for the intramembranous domain. *Biochem. Soc. Trans.* 18:841–843.

Stroud, R. M., and D. A. Agard. 1979. Structure determination of asymmetric membrane profiles using an iterative Fourier method. *Biophys. J.* 25:495–512.